ELSEVIER

Chemical Geology 239 (2007) 138–155

CHEMICAL GEOLOGY
INCLUDING
ISOTOPE GEOSCIENCE

www.elsevier.com/locate/chemgeo

Time scales of formation of zoned magma chambers: U-series disequilibria in the Fogo A and 1563 A.D. trachyte deposits, São Miguel, Azores

Darin C. Snyder [a,*], Elisabeth Widom [a], Aaron J. Pietruszka [b,1], Richard W. Carlson [b], Hans-Ulrich Schmincke [c]

[a] *Department of Geology, Miami University, Oxford, OH 45056-1300, USA*
[b] *Department of Terrestrial Magnetism, Carnegie Institution of Washington, 5241 Broad Branch Road, NW, Washington, DC 20015, USA*
[c] *Fachbereich 4 Geodynamik des Ozeanbodens. IFM-GEOMAR Leibniz Institut für Meereswissenschaften, Wischhofstrasse 1-3, 24148-Kiel, Germany*

Received 8 February 2006; received in revised form 8 November 2006; accepted 7 January 2007

Editor: R.L. Rudnick

Abstract

High precision measurements of ^{226}Ra–^{230}Th–^{238}U disequilibria and Ba concentrations are reported for samples from two chemically zoned trachyte deposits from Fogo volcano, São Miguel, Azores. High-precision U-series disequilibria measurements by plasma ionization multicollector mass spectrometry were performed on pumice lapilli and volcanic glass separates from Fogo 1563 A.D. (~0.14 km^3) and the ~4.7 ka Fogo A (~0.7 km^3) deposits in order to quantify the time scales of magmatic processes. Observed (^{226}Ra)/Ba–(^{230}Th)/Ba relationships in Fogo 1563 are compatible with a conventional instantaneous fractional crystallization model and a pre-eruptive magma residence time of ~50 y. However, the Fogo A data cannot be explained by instantaneous fractional crystallization, and require a prolonged crystallization history. Continuous differentiation models better explain the observed ^{226}Ra–^{230}Th variations within the Fogo deposits and may be more realistic in general. Such models suggest magma residence times prior to eruption of ~50–80 years for Fogo 1563, and ~4.7 ka for the larger volume Fogo A eruption. These time scales represent liquid residence ages rather than the crystallization ages documented in most previous magmatic time scale studies, and allow constraints to be placed on the time scales necessary for the development of chemical zonation within the Fogo magma chamber. Our results indicate that calculated time scales are relatively insensitive to the precise nature of the continuous differentiation models, and further indicate that meaningful magma differentiation time scales can be obtained despite open system behavior, because the Ra–Th disequilibria are overwhelmingly controlled by feldspar fractionation. Calculated time scales are, however, extremely sensitive to D_{Ra}/D_{Ba} ratios. We therefore emphasize the crucial importance to better constrain the relative partitioning of Ra and Ba when employing Ra–Th disequilibrium data to constrain the rates and time scales of igneous processes.

Keywords: U-series disequilibria; Time scales; Magma chamber; Trachyte; Azores

* Corresponding author. 254 Williamsburg Circle, Idaho Falls, ID 83404, USA. Tel.: +1 208 932 4255.
E-mail address: snydesd@gamil.com (D.C. Snyder).
[1] Present address: Department of Geological Sciences, 5500 Campanile Dr., San Diego State University, San Diego, CA 92182, USA.

0009-2541/$ - see front matter © 2007 Elsevier B.V. All rights reserved.
doi:10.1016/j.chemgeo.2007.01.002

1. Introduction

Knowledge of the time scales over which magmas differentiate can be important in the hazard assessment of active volcanoes. However, the rates and duration of magmatic differentiation processes generally remain poorly constrained. Measurements of the disequilibria exhibited among daughter nuclides of the ^{238}U decay series can potentially provide quantitative constraints on the time scales of magma fractionation including crystal growth rates and liquid differentiation time scales (Allegre and Condomines, 1976; Williams et al., 1986; Reagan et al., 1992; Widom et al., 1992; Condomines, 1997; Hawkesworth et al., 2004; Jicha et al., 2005; Reagan et al., 2005; Rogers et al., 2006).

Disequilibrium in the ^{238}U decay series can result from partial melting of mantle peridotite and subsequent separation of crystals from a differentiating magma. Left undisturbed, the decay series nuclides grow back towards radioactive equilibrium, which will be reached after ~5 half-lives ($t_{1/2}$) of the daughter nuclide. ^{238}U decays to ^{230}Th ($t_{1/2}$=75 ka) through three short-lived intermediate daughter nuclides and ^{230}Th decays to ^{226}Ra ($t_{1/2}$=1600 years). Therefore ^{238}U–^{230}Th and ^{226}Ra–^{230}Th disequilibria resulting from U–Th and Th–Ra fractionation will be eradicated in an undisturbed system within ~300 ka and ~8 ka, respectively, following the last chemical fractionation event.

Estimated time scales of magma evolution based on U-series disequilibria studies range from a few centuries to thousands of years for evolved alkaline magmatic systems (Condomines, 1997; Evans, 1999; Hawkesworth et al., 2004), and from less than 10 ka (Volpe and Hammond, 1991; Cooper and Reid, 2003; Reagan et al., 2003) to 100 ka (Charlier and Zellmer, 2000) for evolved calc-alkaline magmatic systems.

Fogo volcano on the island of São Miguel (Azores) has repeatedly erupted strongly compositionally zoned trachyte deposits within the last 10 ka. It thus provides an ideal opportunity to assess residence times and fractionation rates of an evolved magma reservoir by applying U-series disequilibria techniques. The petrogenetic processes operating in the evolution of the Fogo magmas have been well characterized, allowing for magma residence time estimates to be placed in a petrogenetic framework. The available chemical and isotopic data are consistent with closed system fractional crystallization in the development of the Fogo 1563 magmatic system (Watanabe et al., 2005), while minor assimilation has played a role in the development of the Fogo A magmatic system (Snyder et al., 2004). Our high-precision ^{226}Ra–^{230}Th–^{238}U measurements on pumice and glass separates from the two young trachyte deposits provide additional constraints on the time scales of fractionation of evolved alkaline magmatic systems. Magmatic time scale estimates based on crystal ages can be hampered by xenocryst incorporation and complexities in crystal growth histories (e.g. Charlier and Zellmer, 2000). Such potential problems have been avoided in this study through the application of U-series disequilibrium data derived from volcanic glass, the best available proxy for the composition of the differentiating liquid.

2. Geologic setting

The Azores Islands straddle the Mid-Atlantic Ridge (MAR) between 37°–40° N. The island of São Miguel is located near the eastern end of the Azores platform (Fig. 1). São Miguel has three active stratovolcanoes, Sete Cidades, Fogo, and Furnas, that are separated by two fields of Quaternary alkali basalt cinder cones and lava flows (Booth et al., 1978; Moore, 1990). Basalts and trachytes dominate on the islands; intermediate and mixed-magma hybrids are relatively rare, as is common on oceanic islands (Storey et al., 1989; Moore, 1991).

Fogo volcano, in the center of the island (Fig. 1), is composed of >90% trachyte. The oldest dated unit is a 181 ka-old trachytic dome (Gandino et al., 1985). An outer caldera formed between 46 and 26.5 ka, associated with the eruption of approximately 5 km^3 of welded and nonwelded ignimbrites (Moore, 1990). An inner caldera formed at about 15.2 ka resulting in pumice-fall deposits and locally welded ignimbrites with an estimated subaerial volume of 1.5 km^3 (Moore, 1990; Moore, 1991). No eruption took place in the inner caldera until c. 4.7 ka when a large explosive trachyte eruption took place (the Fogo A pumice). The precise age of the Fogo A eruption is, however, uncertain.

Nine radiocarbon ages for the Fogo A trachyte deposit range from 4480 to 5380 y BP with an average of 4936 y BP (Moore and Rubin, 1991; not calibrated to calendar dates). These ^{14}C ages correspond to 5139 to 6158 y BP in calendar years (Reimer et al., 2004). Two additional (uncalibrated) ^{14}C ages of 4435 and 4672 (5086 and 5394 y BP in calendar years) were provided by Shotton et al. (1968, 1969). The overall variation in ^{14}C ages is more than 1000 y for a single eruptive deposit. We suggest that the significant variation in ^{14}C ages is likely due to localized atmospheric ^{14}C dilution caused by outgassing of magmatic CO_2 and resulting in depleted ^{14}C levels in local vegetation. Pasquier-Cardin et al. (1999) have shown that assimilation of ^{14}C-free endogenous CO_2 during photosynthesis has lead to artificial radiocarbon "aging" of modern plants by as

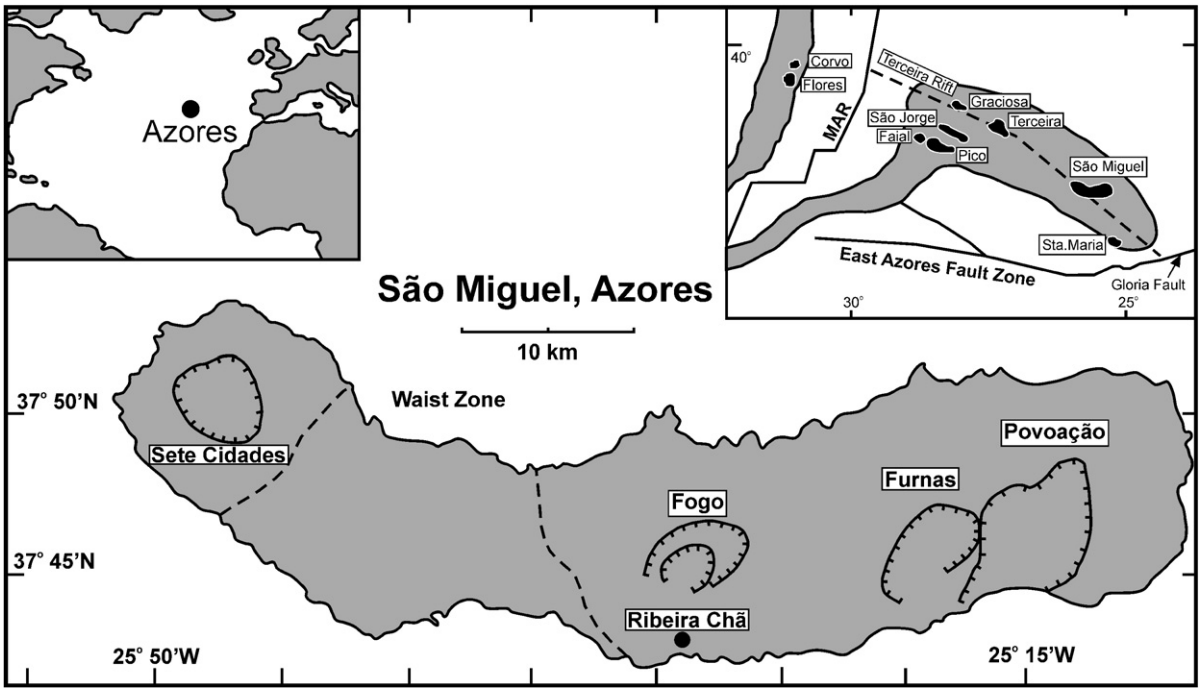

Fig. 1. Map showing the location of the Azores Islands relative to the Mid-Atlantic Ridge (MAR), and a more detailed map of the Island of São Miguel. São Miguel lies near the eastern end of the Azores platform, east of the MAR. The island comprises three large Quaternary stratovolcanoes, Fogo and Furnas (Povoação is extinct) in the east and Sete Cidades in the west (hachured lines mark calderas). The eastern and western stratovolcanoes are separated by two fields of Quaternary alkali basalt cinder cones and lava flows (Waist Zone above). After Moore (1990).

much as 4400 y at Furnas caldera, located on the island of São Miguel <15 km from Fogo volcano. Where vegetation has been affected by magmatic CO_2-uptake, radiocarbon ages will represent minimum ages and will likely be variable. It is thus not possible to quantify the uncertainty associated with these ages. In the case of the Fogo A deposit, the minimum ^{14}C age can be inferred to represent a maximum eruption age; the Fogo A eruption must therefore be <5 ka. Our U-series data further constrain the maximum eruption age to 4.7 ka (Section 4).

Subsequent to the Fogo A eruption, the volcano produced 4 younger trachytic fallout tephra deposits, the youngest erupted in the year 1563 A.D. (Walker and Croasdale, 1970; Booth et al., 1978). In this paper we focus on the Fogo 1563 and Fogo A trachyte pumice tephra deposits.

2.1. Fogo 1563 deposit

The Fogo 1563 deposit amounts to 0.14 km^3 dense rock equivalent (DRE) of chemically zoned trachyte pumice produced during a dominantly plinian eruption (Walker and Croasdale, 1970; Booth et al., 1978). The juvenile material in the deposit consists of fallout ashes interbedded with coarse pumice layers characterized by pale-colored, essentially aphyric angular lapilli (Walker and Croasdale, 1970). Sparse published major and trace element data suggest that the 1563 deposit is compositionally zoned, with an ~1.7-fold variation in highly incompatible elements (e.g. Th=32–54 ppm and U=8–15 ppm), consistent with the variation being produced by ~40% fractional crystallization of sanidine with minor biotite, clinopyroxene, magnetite and apatite (Storey, 1981; Widom et al., 1992; Watanabe et al., 2005). Storey (1981) suggested based on trace element systematics that the Fogo 1563 deposit may have sampled the same evolving trachytic magma body that had produced the older Fogo A trachyte. However, more recent Sr isotopic studies indicate that magma replenishment must have occurred between the two eruptions (Watanabe et al., 2005).

2.2. Fogo A deposit

The Fogo A deposit (Walker and Croasdale, 1970) is dominantly a plinian trachytic fallout tephra (0.6–0.7 km^3 DRE) including some surge and pyroclastic flow deposits (Widom et al., 1992). Our samples were collected from the area around Ribeira Chã. Here, the total thickness of the deposit is about 5 m and can be

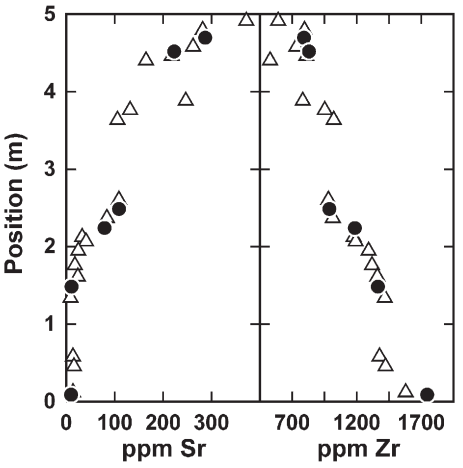

Fig. 2. Relative stratigraphic position of Fogo A whole rock pumice samples versus Sr and Zr concentrations. The filled circles represent samples used to extract the glass separates analyzed in this study, which span much of the range in chemical variations exhibited by the Fogo A deposit. Data from Widom et al. (1992).

divided into two units (for a more detailed discussion see Widom et al., 1992). Unit A is about 3 m thick and comprises 70–80% of the total erupted volume (Walker and Croasdale, 1970). The dominant light colored pumice grades upward into darker and denser pumice (Bursik et al., 1992). The maximum pumice size of 40 cm occurs about 250 cm above the base where syenite xenoliths and banded pumice lapilli first appear (Widom et al., 1992). Unit B, about 1.5 m thick, contains three major surge horizons (Widom et al., 1992). Large syenite xenoliths and banded pumices become abundant about 90 cm above the lowermost surge horizon. The petrogenesis of these xenoliths has been discussed in detail by Widom et al. (1993). The syenites are miarolitic with up to 10% void space. Fresh nodules have subhedral granular textures with interlocking sanidine crystals, whereas hydrothermally altered syenites are subhedral to anhedral granular with sanidine and perthite crystals forming interdigitating boundaries (Widom et al., 1993).

Widom et al. (1992) and Snyder et al. (2004) provide models for the petrogenetic evolution of the Fogo A magmatic system based on chemical, textural, and isotopic data. Major and trace element variations from throughout the stratigraphic extent of the Fogo A deposit indicate that the deposit represents the upper part of a chemically zoned magma chamber erupted from the top down. Fractional crystallization models using the observed phenocryst phases explain the observed chemical zonation via ~70% crystallization combined with <5% bulk assimilation of syenite wall rock.

3. Samples and analytical techniques

In this study, we analyzed a suite of three Fogo 1563 whole rocks and six Fogo A purified glass separates. The Fogo 1563 A.D. samples were only available as powdered whole pumice lapilli, hence whole rock samples were used for this study. However, given the very low crystal content of the pumices (<1% by volume) (this study; Walker and Croasdale, 1970), these samples should closely approximate the liquid compositions.

The 1563 A.D. deposit sample set includes pumice lapilli from the base (ASM-246) and middle (1 m above base, ASM-245) of the deposit collected 5 km southeast of Ribeira Grande, and the top (ASM-244) of the deposit collected 8 km northwest of Furnas. The samples represent the full chemical range of the zoned deposit (SiO_2=61–63 wt.%; Th=30–53 ppm). The deposit becomes progressively less evolved (lower SiO_2, lower Th) upsection.

Widom et al. (1992) report major and trace element chemical compositions for 25 whole rock pumices from the Fogo A deposit. SiO_2, Na_2O, Al_2O_3 and CaO each

Table 1
Trace element abundances for Hawaiian rock standard Kil1919

	Ba ($\mu g\ g^{-1}$)	Th ($\mu g\ g^{-1}$)	U ($\mu g\ g^{-1}$)	Sr ($\mu g\ g^{-1}$)	Nd ($\mu g\ g^{-1}$)	Sm ($\mu g\ g^{-1}$)	Yb ($\mu g\ g^{-1}$)
Kil1919 #4[a]	134.6	1.220	0.4255	394.1	24.67	6.099	2.026
Kil1919 #5[a]		1.221	0.4258				2.028
Kil1919 #6[a]	134.6	1.221	0.4264	393.9	24.70	6.105	
Kil1919 #7[a]	135.7	1.228	0.4279	395.3	24.84	6.140	2.039
Average	135.2	1.225	0.4272	394.6	24.77	6.123	2.039
% 2σ	0.94	0.60	0.50	0.38	0.73	0.72	0.69
Literature[b]	135.3			398.2			

[a]These analyses were performed by A. Pietruszka during the course of the current study and are reported in Pietruszka et al. (2006).
[b]Average of five XRF analyses reported by Rhodes (1996).

vary by 2–5 wt.% and correlate with stratigraphic position, with the deposit becoming more mafic upsection. The whole rock trace element concentrations vary widely with Zn, Rb, Y, Zr, Nb, Th and U exhibiting incompatible behavior, and Cr, Sr and Ba exhibiting compatible behavior. Zr and Sr concentrations range from 1745–529 and 372–9 ppm, respectively (Fig. 2). The subset of samples selected for this study range in Zr and Sr concentrations from 1745–791 and 372–9 ppm, respectively, thus providing a reasonable representation of the compositional variation of the deposit as a whole.

Fogo A glass was separated from individual pumice lapilli by hand picking under a binocular microscope, avoiding apparent impurities. No secondary alteration products were observed in any of the materials. Glass separates were rinsed in methanol then cleaned with 2 N HCl for 10 min in an ultrasonic bath followed by a rinse in high-purity water in order to remove any adhering salts prior to dissolution (Snyder et al., 2004).

All chemical separations and isotopic measurements were done at the Department of Terrestrial Magnetism. The procedures used were described by Pietruszka et al. (2002), with the exception that the Th and U cuts for isotopic composition were passed through a second 50-µl column of Eichrom TRU (TransUranic) Resin to remove potential high-mass hydrocarbon interferences. In addition to the ^{233}U, ^{229}Th and ^{228}Ra spikes described by Pietruszka et al. (2002), all dissolved samples were spiked with ^{135}Ba, ^{173}Yb, ^{84}Sr, ^{85}Rb, and a mixed ^{149}Sm–^{150}Nd spike for concentration measurements by isotope dilution. Separation of Rb, Sr, Yb, Ba and rare-earth elements from the rock matrix was

Table 2
Elemental concentrations and isotopic compositions of samples from the Fogo 1563 and Fogo A trachyte deposits

	Fogo A glass separates						Fogo 1563 whole rocks		
	ASM-220	ASM-210	ASM-205	ASM-201	ASM-204	ASM-218	ASM-244	ASM-245	ASM-246
Position (m)	0.09	1.51	2.28	2.53	4.60	4.78	Base	~1	top
SiO_2 wt.%[a]	62.9	62.8	62.7	61.9	59.5	60.9	62.8	61.8	60.9
[Ba] µg g^{-1}	0.6517	3.214	71.66	134.7	338.7	137.4	20.59	74.48	125.8
[Sr] µg g^{-1}[b]	0.6816	1.692	22.55	45.22	178.5	57.57	9.764	25.46	29.94
[Rb] µg g^{-1}[b]	387.3	260.3	216.3	162.4	143.2	152.6	343.5	225.8	216.7
[U] µg g^{-1}	18.80	11.19	7.790	6.282	4.589	5.694	14.29	8.352	8.149
[Th] µg g^{-1}[b]	67.65	41.20	29.38	23.25	18.03	20.72	52.51	30.83	29.92
[Nd] µg g^{-1}[b]	134.6	109.4	83.89	73.78	60.89	69.32	135.4	98.14	95.31
[Sm] µg g^{-1}	22.37	17.23	13.35	11.88	10.02	11.20	21.60	15.72	15.40
[Yb] µg g^{-1}	9.475	6.355	4.762	4.085	3.203	3.829	9.059	5.945	5.810
^{87}Sr/^{86}Sr[b]	0.705214	0.705071	0.704895	0.704948	0.704841	0.704895			
^{143}Nd/^{144}Nd[b]	0.512785	0.512767	0.512760	0.512760	0.512773	0.512756			
[^{226}Ra] fg g^{-1}	5951	3655	2677	2075	1546	1895	1353	959	987
$\pm 2\sigma_m$	43	35	18	20	15	14	8	8	7
(^{238}U/^{232}Th)[b]	0.8433	0.8239	0.8047	0.8200	0.7723	0.8339	0.8257	0.8220	0.8264
(^{230}Th/^{238}U)	1.0345	1.0605	1.0873	1.0681	1.1388	1.0534	1.0706	1.0737	1.0677
(^{230}Th/^{232}Th)	0.8724	0.8738	0.8750	0.8758	0.8795	0.8784	0.8840	0.8826	0.8823
(^{234}U/^{238}U)[b]	0.9995	1.0022	1.0020	1.0015	1.0005	0.9999	1.0008	1.0031	1.0019
(^{226}Ra/^{230}Th)	0.9066	0.9128	0.9363	0.9161	0.8763	0.9358	0.2620	0.3167	0.3362
$\pm 2\sigma$	0.0046	0.0054	0.0046	0.0055	0.0053	0.0049	0.0012	0.0017	0.0018
Eruption age corrected[c]									
(^{230}Th/^{232}Th)$_o$[b]	0.8737	0.8759	0.8780	0.8783	0.8843	0.8804	0.8843	0.8828	0.8826
$\pm 2\sigma$	0.0032	0.0032	0.0032	0.0032	0.0032	0.0032	0.0032	0.0032	0.0032
(^{230}Th/^{238}U)$_o$	1.0360	1.0632	1.0911	1.0711	1.1449	1.0558	1.0709	1.0740	1.0680
$\pm 2\sigma$	0.0043	0.0044	0.0045	0.0044	0.0047	0.0044	0.0044	0.0044	0.0044
(^{226}Ra/^{230}Th)$_o$	0.2741	0.3142	0.4867	0.3373	0.0163	0.4924	0.1077	0.1738	0.1974
$\pm 2\sigma$	0.0016	0.0021	0.0026	0.0023	0.0006	0.0027	0.0005	0.0009	0.0010
(^{226}Ra)$_o$/Ba	6.068	0.8613	0.0428	0.0125	0.0002	0.0160	0.0593	0.0155	0.0101
(^{230}Th)$_o$/Ba	22.1412	2.7409	0.0879	0.0370	0.0115	0.0324	0.5506	0.0892	0.0513

[a] Measured whole rock SiO_2 concentration for Fogo A whole rock samples from Widom et al. (1992).

[b] Data for Fogo A glass separates from Snyder et al. (2004).

[c] Measurements were made in 2001 and eruption ages used for these corrections are 438 y and 4700 y prior to the analyses for the Fogo 1563 A.D. and Fogo A eruptions, respectively. Decay constants used for eruption-age corrected activities are: λ^{238}U (1.551×10^{-10} year^{-1}), λ^{232}Th (4.948×10^{-11} year^{-1}), λ^{230}Th (9.158×10^{-6} year^{-1}), and λ^{226}Ra (4.332×10^{-4} year^{-1}). Uncertainties on age corrected activity ratios do not include propagated errors on the eruption age. See text for explanation.

accomplished by drying down the first 4.6 ml of 1.5 N HNO_3 collected from the Th–U TRU Resin columns followed by dissolution in 2 ml of 1.25 N HCl. These solutions were then passed through AG50W-X8 resin columns in a procedure similar to that detailed by Pietruszka et al. (2006).

Barium, Rb, Nd, Sm, and Yb concentrations by isotope dilution were measured on a VG-P54 multi-collector ICP-MS, and Sr concentrations by isotope dilution were measured on a VG-354 thermal ionization mass spectrometer. The Th, U and Ra concentrations and isotope ratios were also measured on a VG-P54, using the high-precision isotope dilution MC-ICP-MS technique described by Pietruszka et al. (2002). With the exception of Ra, we estimate a precision of ±<1% 2σ on measured concentrations of these elements based on replicate analyses of the rock standards Kil1919 (Table 1) and Table Mountain Latite (TML) (Jar #3). ^{226}Ra concentration and Th/U, (^{234}U/^{238}U) and (^{230}Th/^{232}Th) ratio measurements of the Pliocene rock standard TML (Jar #3) provide an average and long-term reproducibility of 3609 (fg g^{-1})±0.8%, 2.827±0.06%, 1.0007±0.19% and 1.0736±0.23% 2σ, respectively (Pietruszka et al., 2002). However, the precision of ^{226}Ra concentration measurements is often sample limited and therefore we use the individual in-run errors on the ^{226}Ra measurements.

4. Results

Table 2 shows the results of ^{238}U–^{230}Th–^{226}Ra disequilibria, and precise determinations of Ba, Sr, Rb, U, Th Nd, Sm, and Yb abundances for whole rocks and purified glasses from the Fogo 1563 and Fogo A chemically zoned volcanic deposits. Eruption age corrected values (438 y BP for Fogo 1563 and 4700 y BP for Fogo A) for (^{230}Th/^{232}Th)$_o$, (^{230}Th/^{238}U)$_o$ and (^{226}Ra/^{230}Th)$_o$ (parentheses denote activity ratio) are shown in Table 2. Based on the assumption that the ^{14}C ages represent ages older than the actual eruption age for the Fogo A deposit and constraints placed on the maximum eruption age by our U-series disequilibrium data (discussed later), we have used an eruption age of 4700 for the Fogo A deposit. Correcting the (^{226}Ra/^{230}Th) to the maximum possible eruption age of Fogo A provides a minimum calculated magma residence time.

The Fogo 1563 whole rocks display wide ranges in Ba and Sr concentrations (20–126 ppm and 10–30 ppm, respectively) and more modest ranges in U and Th concentrations (8–14 ppm and 30–52 ppm, respectively), with samples becoming systematically less evolved (higher Ba and Sr) upsection. A similar relationship is observed in the Fogo A deposit; all reported trace element concentrations in the Fogo A glass separates display variations correlated with both stratigraphic position and wt.% SiO_2 (Fig. 3). Both Sr and Ba display dramatic decreases in concentration (339–<1 ppm and 178–<1 ppm, respectively) with increasing wt.% SiO_2, while Th and U increase in concentration (18–68 ppm and 5–19 ppm respectively) with increasing wt.% SiO_2. Recent work shows constant ^{87}Sr/^{86}Sr ratios (0.70500± 2) throughout the Fogo 1563 A.D. deposit (Watanabe et al., 2005), in contrast to the Fogo A deposit, which shows significant variability in ^{87}Sr/^{86}Sr ratios (0.70484

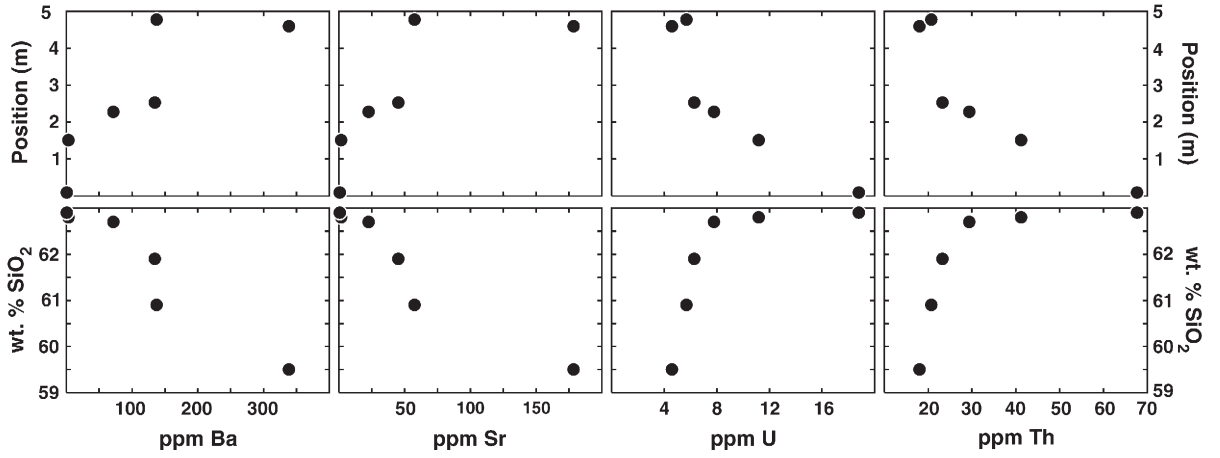

Fig. 3. Trace element concentrations of glass separates versus stratigraphic position within the Fogo A deposit and versus wt.% SiO_2. The most evolved samples are located near the bottom of the deposit with the samples becoming less evolved towards the top of the deposit. Both Sr and Ba concentrations decrease with increasing SiO_2, while Th and U concentrations increase with increasing SiO_2. This zonation is interpreted to approximate the inverse compositional zonation of the pre-eruptive magma chamber.

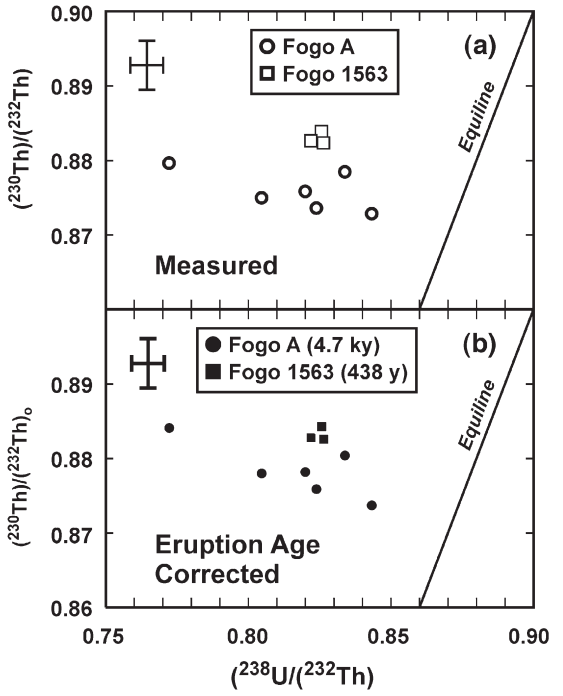

Fig. 4. U–Th isotope equiline diagram with both the Fogo 1563 and Fogo A samples. A representative error bar is shown in the upper left of each plot. (a) Measured values for Fogo 1563 samples show no variation in either (^{230}Th/^{232}Th) or (^{238}U/^{232}Th). Measured values for Fogo A samples do not vary outside of analytical uncertainty in (^{230}Th/^{232}Th) but do vary in (^{238}U/^{232}Th). (b) Eruption age corrected values for Fogo 1563 samples show no variation in either (^{230}Th/^{232}Th)$_o$ or (^{238}U/^{232}Th). However, eruption age corrected values for Fogo A samples do vary in both (^{230}Th/^{232}Th)$_o$ and (^{238}U/^{232}Th). Variations in (^{230}Th/^{232}Th)$_o$ are attributed to assimilation combined with fractional crystallization (Snyder et al., 2004). Therefore, Th–Ra disequilibrium data are required to address differentiation time scales.

to 0.70521 in leached glass separates, Snyder et al., 2004).

Fogo 1563 whole rock (^{234}U/^{238}U) ratios are all 1.000±0.003, consistent with expected magmatic values and indicating that post-eruptive alteration has not disturbed the U isotopic compositions. (^{238}U/^{232}Th) and (^{230}Th/^{232}Th) do not vary outside of analytical uncertainty (0.822–0.826 and 0.882–0.884, respectively; Fig. 4), while (^{226}Ra/^{230}Th) vary from 0.262 in the most evolved to 0.336 in the least evolved sample. Eruption age corrected values are reported in Table 2.

Fogo A glass separate (^{234}U/^{238}U) ratios are all 1.000±0.002. (^{238}U/^{232}Th) ratios range from 0.772 for the least evolved sample to 0.843 for the most evolved sample. Measured (^{230}Th/^{232}Th) ratios do not vary outside of analytical uncertainty, however (^{230}Th/^{232}Th)$_o$ ratios generally decrease with increasing (^{238}U/^{232}Th) (Fig. 4). Measured (^{226}Ra/^{230}Th) ratios vary from 0.876–0.936, with age-corrected (^{226}Ra/^{230}Th)$_o \ll 1$. The eruption age corrected values are obviously controlled by the age used in the correction (see above discussion concerning ^{14}C ages). Note, however, that the (^{226}Ra/^{230}Th) provides a maximum eruptive age independent of ^{14}C, because (^{226}Ra/^{230}Th)$_o$ must be ≥ 0. The measured (^{226}Ra/^{230}Th) of ASM-204 therefore provides a maximum eruption age for the Fogo A deposit of 4.73 ka. Samples from both the Fogo 1563 and Fogo A deposits exhibit apparent positive linear correlations of (^{226}Ra)$_o$/Ba and (^{230}Th)$_o$/Ba (r^2=0.9990 and 0.9998 respectively) (Fig. 5).

5. Discussion

5.1. Fogo 1563

The chemical variations exhibited by the Fogo 1563 whole rocks can be explained by 43% crystallization of

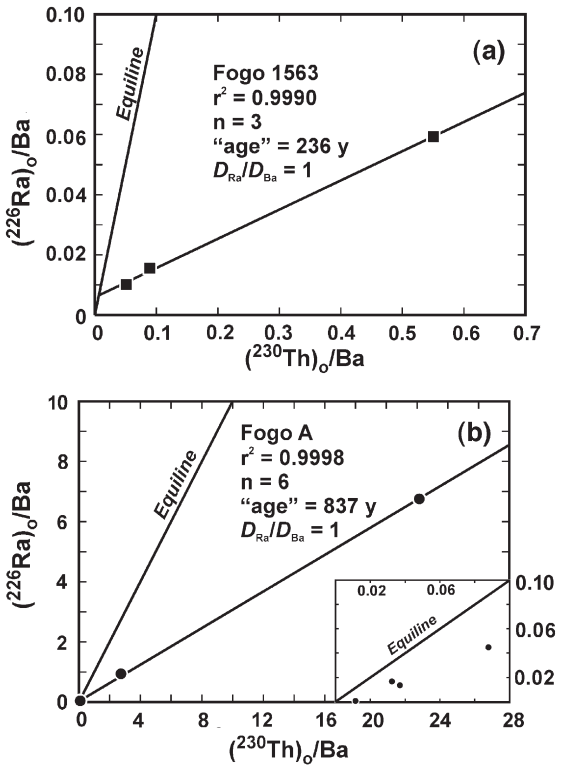

Fig. 5. Ra–Th equiline diagrams for the (a) Fogo 1563 and (b) Fogo A samples. Both sample sets exhibit linear relationships (r^2>0.99). The inset in (b) shows the four samples with the lowest (^{226}Ra)$_o$/Ba and (^{230}Th)$_o$/Ba ratios. The "ages" listed for the respective deposits assume instantaneous crystallization during which Ra and Ba were equally partitioned into the fractionating assemblages. Note the significant misfit of this model to the low (^{226}Ra)$_o$/Ba samples in the inset in (b).

a sanidine-dominated (91%) assemblage with minor biotite (0.5%), clinopyroxene (4.7%), magnetite (3.7%) and apatite (0.7%). Constant $^{87}Sr/^{86}Sr$ ratios throughout the deposit are consistent with evolution of the magma by closed system fractional crystallization (Watanabe et al., 2005). The lack of variation in $(^{238}U/^{232}Th)$ or $(^{230}Th/^{232}Th)_o$ among the Fogo 1563 samples, however, precludes the use of U–Th disequilibrium data for constraining the time scales of magmatic differentiation (Fig. 4). The consistency in $(^{238}U/^{232}Th)$ suggests that U–Th fractionation within the magma was extremely minor and thus no variation in $(^{230}Th/^{232}Th)_o$ would be expected regardless of the amount of time since fractionation occurred, or the magma residence "age".

$(^{226}Ra/^{230}Th)_o$ ratios in the Fogo 1563 samples are variable and $\ll 1$ (Table 2), providing an opportunity to investigate the time scales of magmatic differentiation through the application of Th–Ra disequilibrium data. Ra possesses neither a relatively long-lived nor a stable isotope necessary for normalization on an isochron diagram. Therefore, in order to infer time scale information one must utilize an element with partitioning behavior similar to Ra such as Ba (Williams et al., 1986). If one assumes instantaneous Th–Ra fractionation with respect to the half-life of Ra and $D_{Ra}=D_{Ba}$ during crystallization, a differentiation age of ~240 y prior to eruption is required for the Fogo 1563 magma, with no continued fractionation (Fig. 5a). This instantaneous fractionation model would, however, require hundreds of years of static behavior with no fractionation, which is impossible in view of constant heat loss of the resident magma and ensuing crystallization. Furthermore, Ra and Ba are generally fractionated from one another, as well as from Th, in chemically evolved magmatic systems (Zellmer et al., 2000; Cooper et al., 2001). A more plausible model, and the resulting magmatic fractionation time scale, is discussed below.

5.1.1. Partition coefficients

The relative partitioning of Ra and Ba can be assessed by modeling the bulk D_{Ba} during fractional crystallization, then calculating a corresponding bulk D_{Ra} based on the ionic radii of Ba and Ra, the size of the cation site in fractionating minerals, and the elastic modulus of the site for a given temperature, pressure and composition (Blundy and Wood, 1994). The bulk D_{Ba} in the Fogo 1563 deposit has been quantified based on the variations in abundance of the highly incompatible element Th. The fractionating assemblage is composed dominantly of sanidine, in which Th is expected to behave extremely incompatibly (Mahood and Hildreth, 1983). We have calculated $D_{Th}=0.004$ using the fractionating assemblage provided by Widom et al. (1992) and partitioning data from Mahood and Hildreth (1983) and Bourdon et al. (1994). The Th abundance variations in the Fogo 1563 whole rocks require 43% fractional crystallization, for which a bulk D_{Ba} of 4.22 is required to produce the observed variations in Ba in the Fogo 1563 trachyte suite.

The behavior of Ra and Ba during fractional crystallization of the Fogo 1563 magma is overwhelmingly dominated by sanidine fractionation. Blundy and Wood (2003) presented an equation that allows the relative partitioning of two isovalent cations to be predicted:

$$D_a = D_b \times \exp\left[\frac{-910.17E_M^{n+}}{T}\left\{\frac{r_{0(M)}^{n+}}{2}\left(r_b^2-r_a^2\right)-\frac{1}{3}\left(r_b^3-r_a^3\right)\right\}\right]$$

where D_a is the distribution coefficient for element a (radius r_a) in the phase of interest at a given set of pressure, temperature and melt composition conditions; D_b is the known distribution coefficient for an isovalent cation b (radius r_b) in the phase of interest at a given set of pressure, temperature and melt composition conditions; E is Young's Modulus of the host crystal; $r_{0(M)}$ is strain-free or ideal cation radius; and T is the temperature in Kelvin. Uncertainty in the calculated D_{Ra}/D_{Ba} ratio is primarily a function of the uncertainty in the ideal (strain-free) cation radius of the M-site in alkali feldspar. We have calculated the ideal strain-free radius based on the relationship between X_{Or} and $r_{0(M)}$ from Blundy and Wood (2003). Although this relationship is only strictly valid for specific temperature (650–750 °C) and pressure (0.2 GPa) conditions that are different from those in the Fogo magma (T=950 °C; Wolff and Storey, 1983), the D_{Ba} calculated using the above relationship models the observed variations of Ba in the Fogo trachytes reasonably well considering the predicted increase in compatibility with increase in temperature described by Blundy and Wood (2003). The paucity of experimentally determined cation radii of the M-site in alkali feldspar over a range of orthoclase compositions and temperature and pressure conditions adds uncertainty to the D_{Ra}/D_{Ba} ratio in the Fogo magmatic system. Nevertheless, we have calculated $r_{0(M)}=1.43$ Å based on the relationship described by Blundy and Wood (2003; Eq. (35)) using a sanidine composition of $X_{Or}=0.41$ (Widom et al., 1992). The model presented by Blundy and Wood (2003) predicts a bulk D_{Ra} of 1.95 and a corresponding $D_{Ra}/D_{Ba}=0.34$ in a fractionating assemblage dominated by sanidine. The values used in this calculation are presented in Table 3.

Table 3
Variables used to predict the D_{Ra}/D_{Ba} ratio in sanidine for the Fogo 1563 and Fogo A samples

	Fogo 1563	Fogo A
E_m [a]	101.9 (GPa)	101.9 (GPa)
$r_{0(M)}$ [b]	1.43 Å	1.43 Å
$r_b = r_{Ba}$	1.52 Å	1.52 Å
$D_b = D_{Ba}$	4.22	5.67
T	1223 K	1223 K
$r_a = r_{Ra}$	1.59 Å	1.59 Å

[a] Young's modulus calculated using Eqs. (4) and (6) of Blundy and Wood (2003).
[b] Ideal strain-free cation radius calculated using Eq. (35) of Blundy and Wood (2003).

The relative partitioning of Ra and Ba calculated here is contrary to the previous suggestion of Hawkesworth et al. (2000) that Ra may be *more* compatible than Ba in sanidine. The difference between our predictions and those of Hawkesworth et al. (2000) of the relative partitioning of Ra and Ba in sanidine is likely due to the value used for the ideal cation radius in the lattice strain model of Blundy and Wood (1991). According to the lattice strain model, during partitioning involving two homovalent cations, the cation whose ionic radius is more similar to the ideal cation radius (r_0) will be preferentially incorporated into the crystal structure (i.e. more compatible/less incompatible). The radius of Ba^{2+} (X-fold coordination = 1.52 Å; Shannon, 1976) is more similar to the ideal strain-free radius calculated above (1.43 Å) than is the radius of Ra^{2+} (X-fold coordination = 1.59 Å; estimated from Shannon, 1976). However, if r_0 is assumed to be 1.59 Å, then $D_{Ra}/D_{Ba} = 1.27$. This would have a large effect (order of magnitude) on calculated time scales as will be discussed in Sections 5.1.2 and 5.2.1.

Given $D_{Ra}/D_{Ba} < 1$, as calculated for the Fogo magmas, instantaneous fractionation would cause an initial increase in Ra/Ba ratios in more fractionated magmas. For $D_{Ra}/D_{Ba} = 0.34$, the calculated time since instantaneous fractionation (compared to a model in which $D_{Ra} = D_{Ba}$), would be only ~50 y rather than ~240 y prior to eruption, to explain the measured (^{226}Ra) and (^{230}Th) data (Fig. 6a).

5.1.2. Fogo 1563 time scale modeling

An instantaneous fractionation model is unrealistic because it requires that fractionation occurred and then ceased for tens of years before eruption, yet the magma should continue to cool and crystallize. Thus, models involving continuous fractionation (e.g. Blake and Rogers, 2005; Johansen et al., 2005) are more realistic. We have therefore developed models to describe the observed (^{226}Ra)–(^{230}Th)–Ba variations in the Fogo deposits that approximate continuous fractionation. These models assume continuous replenishment of the magma chamber by new batches of relatively less evolved magma through time, with a constant composition equal to that of our least evolved sample. Each new batch of magma is allowed to crystallize subsequent to emplacement while radioactive ingrowth and

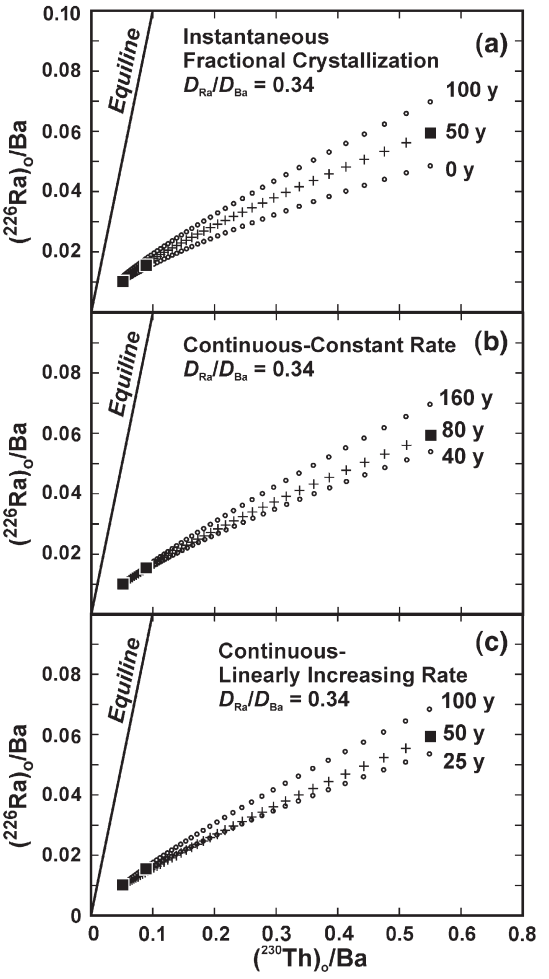

Fig. 6. Th–Ra isotope equiline diagram for the Fogo 1563 samples. Filled squares are the measured values corrected to time of eruption, crosses represent best-fit model results, and open circles represent model results for other time scales shown for comparison. Fractional crystallization increments of 0.01% were used in the models, but only 1% fractional crystallization increments are illustrated. (a) The three modeled paths illustrated in the instantaneous fractional crystallization plot represent instantaneous crystallization followed by 0, 50 and 100 years for radioactive ingrowth/decay. (b) The continuous model with a constant rate of crystallization (crosses) requires a fractionation time of 80 y. (c) The continuous model with a linearly increasing rate of crystallization (crosses) suggests a crystallization duration of 50 y. Note the similarity in modeled time scales between the instantaneous and both continuous fractionation models.

decay occur such that the first magma batch injected into the chamber will be the most chemically and isotopically evolved magma at the end of the model. This model assumes no physical mixing between the newly introduced magmas and those already in the magma chamber (i.e. chemical and isotopic zonation is maintained). The initial batch of magma undergoes the required net amount of crystallization over an extended period of time, fit such that at the final crystallization step the (^{226}Ra)–(^{230}Th)–Ba is appropriate for the value measured in the most evolved pumice. In this model, the least evolved magma is emplaced in the chamber just prior to eruption whereas the most evolved magma has resided in the chamber for the full duration. The period of time over which any individual batch of magma is affected by radioactive ingrowth and decay is dependent upon how long the magma has resided in the chamber.

This model allows continuous-constant rate fractional crystallization conditions to be simulated using small crystallization increments with "sit" time between each crystallization increment allowing for radioactive ingrowth and/or decay of ^{238}U, ^{230}Th and ^{226}Ra. The duration of "sit" time between each crystallization increment is a function of the total elapsed time of the model and size of fractional crystallization increment.

We have used 0.01% fractional crystallization increments (10,000 steps), because models with a minimum of one thousand steps are required to adequately simulate continuous fractionation. Increasing the number of steps in our model does not affect the calculated duration of crystallization, whereas models with fewer than one thousand steps produce slightly longer calculated crystallization durations. Using the calculated $D_{Ra}/D_{Ba}=0.34$ this model provides a time scale of differentiation of 80 y prior to eruption (Fig. 6b), with a fractionation rate of 0.005/y. The degree to which this time scale is dependent on D_{Ra}/D_{Ba} (and ultimately dependent on the ideal strain-free cation radius used in the lattice strain model) is significant. $D_{Ra}/D_{Ba}=1$ results in an approximately one order of magnitude longer duration of fractionation.

A continuous fractionation model in which the rate of crystallization linearly increases (envisioning more rapid crystallization as the magma chamber decreases in size and/or the magma rises to a shallower level in the crust) has also been evaluated. The rate of crystallization in this model increases from 0.006/y at the first crystallization step up to ~0.017/y at the final crystallization step. In this case, the model provides a predicted duration of fractionation of 50 y (Fig. 6c). The instantaneous and continuous constant rate and linearly increasing rate fractional crystallization models are all in good agreement with the measured values on the Fogo 1563 whole rocks, although an instantaneous fractional crystallization model requires ~50 y between the cessation of crystallization and eruption, which is unrealistic. The continuous models suggest rapid crystallization in which the Fogo 1563 magma chamber became chemically zoned with ~43% crystallization over a period of only 50–80 y prior to eruption.

5.2. Fogo A

The chemical variation between the least and most evolved Fogo A trachytes could be produced by 70–75% crystallization (88% sanidine, 4% biotite, 3% clinopyroxene, 1% apatite, 1% oxide and 0.05% zircon) of the observed phenocryst assemblage (Widom et al., 1992). Snyder et al. (2004) further refined this model having identified both Sr and Th isotopic variations within the Fogo A deposit. The observed Sr and Th concentration and isotopic variations in the glasses are suggested to have developed as a result of ~69% crystallization combined with ~5% bulk assimilation of the syenite wall rock ($r=0.075$) (where r represents the rate of assimilation/the rate of crystallization) (Fig. 7).

Unlike the Fogo 1563 deposit, the Fogo A glass samples vary in both (^{238}U/^{232}Th) and (^{230}Th/^{232}Th)$_o$ (Fig. 4). However, U–Th disequilibrium data alone do not provide meaningful chronological information; the negative correlation of (^{238}U/^{232}Th) with (^{230}Th/^{232}Th)$_o$ is opposite than expected if this was an isochronous relationship. This relationship instead is interpreted as a relict of combined assimilation and fractional crystallization (AFC) processes active in the pre-eruptive Fogo A magma chamber (Snyder et al., 2004). However, all of the Fogo A glass separates possess (^{226}Ra/^{230}Th)$_o$ ratios that are <1 and variable, thus providing a potential tool for constraining pre-eruptive time scales.

5.2.1. Fogo A time scale modeling

It is possible to model the Fogo A data using a similar approach to that of the Fogo 1563 A.D. data. If we assume a bulk $D_{Th}=0.004$, the Th abundance variations in the Fogo A glass separates require ~74% fractional crystallization of a fractionating assemblage dominated by sanidine, consistent with the fractional crystallization model proposed by Widom et al. (1992). The observed variations in Sr and Ba concentrations thus require bulk D's of 5.19 and 5.67, respectively for the Fogo A glass suite (Fig. 8). The continuous fractional crystallization model employing a constant rate of fractional crystallization (0.0002/y), bulk $D_{Ba}=5.67$ and $D_{Ra}/D_{Ba}=0.34$, would require a time scale of fractionation of 3.5 ky, but

produces a poor fit to the measured data (Fig. 9). The continuous fractional crystallization model using a linearly increasing rate of fractional crystallization (0.00009 to 0.0003/y) predicts a duration of fractionation of 4.7 ky (Fig. 9).

However, Snyder et al. (2004) demonstrated based on the Sr and Th isotopic compositions of the Fogo A glasses that assimilation of syenite wall rock played a role in the evolution of the Fogo magma chamber. Thus, a model including assimilation of syenite wall rock is more appropriate than the prolonged closed system fractional crystallization models. This model assumes bulk assimilation of "old" syenite wall rock [i.e. (^{226}Ra/^{230}Th)=1] because many syenites have model ages >8 ka (Widom et al., 1993). Based on the chemical data presented by Widom et al. (1993), the model assumes a Ba/Th ratio in the assimilant of 0.5. Using a bulk D_{Ra}/D_{Ba}=0.34, and the assimilation parameters of Snyder et al. (2004) (Fig. 7), results of the continuous fractionation model with assimilation-fractional crystallization (AFC) using a linearly increasing rate of AFC still suggest that 4.7 ky were required for the chemical and isotopic variations of the Fogo A magma chamber to develop (Fig. 9). This suggests that assimilation likely had a negligible effect on the calculated magma residence ages.

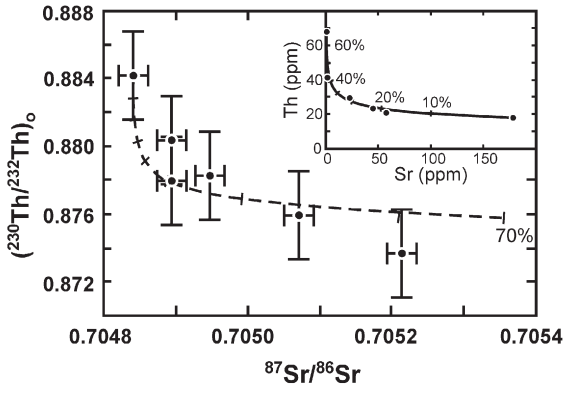

Fig. 7. AFC models with syenite wall rock (dashed) as the assimilant. Tick marks represent percent crystallization. Approximately 69% crystallization is required to account for the observed Th and Sr concentration (inset) and isotopic variation in the Fogo A trachytic glasses. The solid line in the inset is the AFC path for both syenite and sediment. The tick marks in the inset represent percent (10% increments) crystallization using syenite as the assimilant. Assimilation of sediment results in slightly lower Th/Sr ratios for given percentage of crystallization. Input parameters: least evolved, uncontaminated Fogo A magma, 18.03 ppm Th, 178.5 ppm Sr, ^{87}Sr/^{86}Sr=0.70484, (^{230}Th/^{232}Th)=0.8841; contaminating syenite, 40 ppm Th, 10 ppm Sr, ^{87}Sr/^{86}Sr=0.70620, (^{230}Th/^{232}Th)=0.8100; D_{Sr}=6; D_{Th}=0.001; r=0.075. After Snyder et al. (2004).

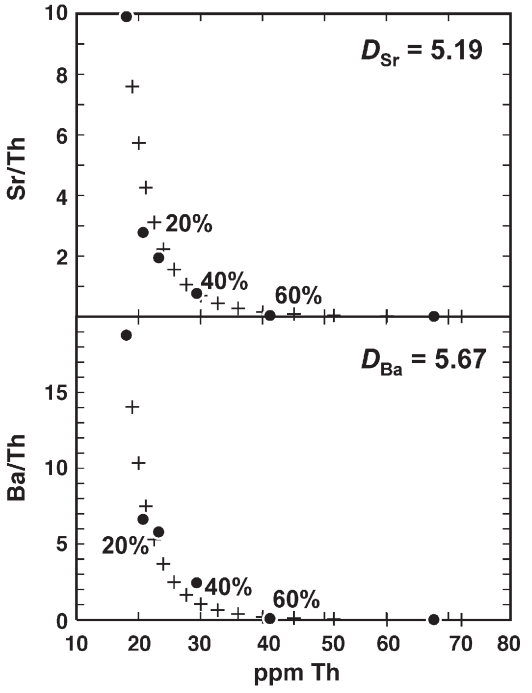

Fig. 8. Ba/Th and Sr/Th ratios versus Th concentrations for Fogo A illustrating the consistency of the factional crystallization model with the measured data. Bulk distribution coefficients used are: Th=0.004; Sr=5.19; Ba=5.67. Tick marks represent 5% fractional crystallization.

5.2.2. Sensitivity of model to variable input parameters

The modeled pre-eruptive residence time of the Fogo A magma is partially controlled by the eruption age used to correct the measured (^{226}Ra) and (^{230}Th) values. Because the precise eruption age for the Fogo A deposit is poorly constrained, we have calculated the duration of differentiation assuming three different eruption ages (Fig. 10). Each of the model curves in Fig. 10 are generated using our preferred continuous-linearly increasing rate of AFC model illustrated in Fig. 9. The slope of the age corrected data becomes steeper with younger assumed eruption ages, in turn requiring longer durations of differentiation. The assumed 4.7 ka eruption age used in the previous calculations thus provides a *minimum* estimate of the pre-eruptive magma residence time.

The modeled time scale of differentiation is relatively insensitive to variable AFC input parameters. Table 4 illustrates the results of variable (^{226}Ra/^{230}Th) ratios of the assimilated syenite as well as variable rates of assimilation relative to fractional crystallization (denoted as "r-value"). Assimilation of young syenites or potential melts of syenites with (^{226}Ra/^{230}Th)≠1 will only have a modest effect on the estimated time scale of fractionation. A two-fold decrease or increase in the

(^{226}Ra/^{230}Th) ratio of the assimilant only changes the magma residence time by 300–500 y (~6–10%). A ten-fold decrease in the (^{226}Ra/^{230}Th) ratio of the assimilant only results in a 500 y (~10%) increase in the modeled time scale. A ten-fold increase in the (^{226}Ra/^{230}Th) ratio of the assimilant cannot explain the data (Fig. 11). Changing the *r*-value also results in only modest changes in calculated time scales. Halving the *r*-value results in no change in the calculated time scale and doubling the *r*-value results in only a 200 y (~4%) increase. A ten-fold increase in the rate of assimilation relative to fractional crystallization (r=0.75; an extremely high ratio) results in a modeled time scale of differentiation of ~18,000 y, but produces an extremely poor fit to the data (Fig. 11). The model results in Table 4 illustrate the modest effect that a wide range in AFC parameters have on our modeled time scales.

The model is most sensitive to the assigned *D*-values. Fig. 12 illustrates the results of the continuous AFC model using various D_{Ra}/D_{Ba} ratios. A two-fold increase or decrease in the D_{Ra}/D_{Ba} ratio results in a corresponding ~3-fold increase or decrease in the modeled

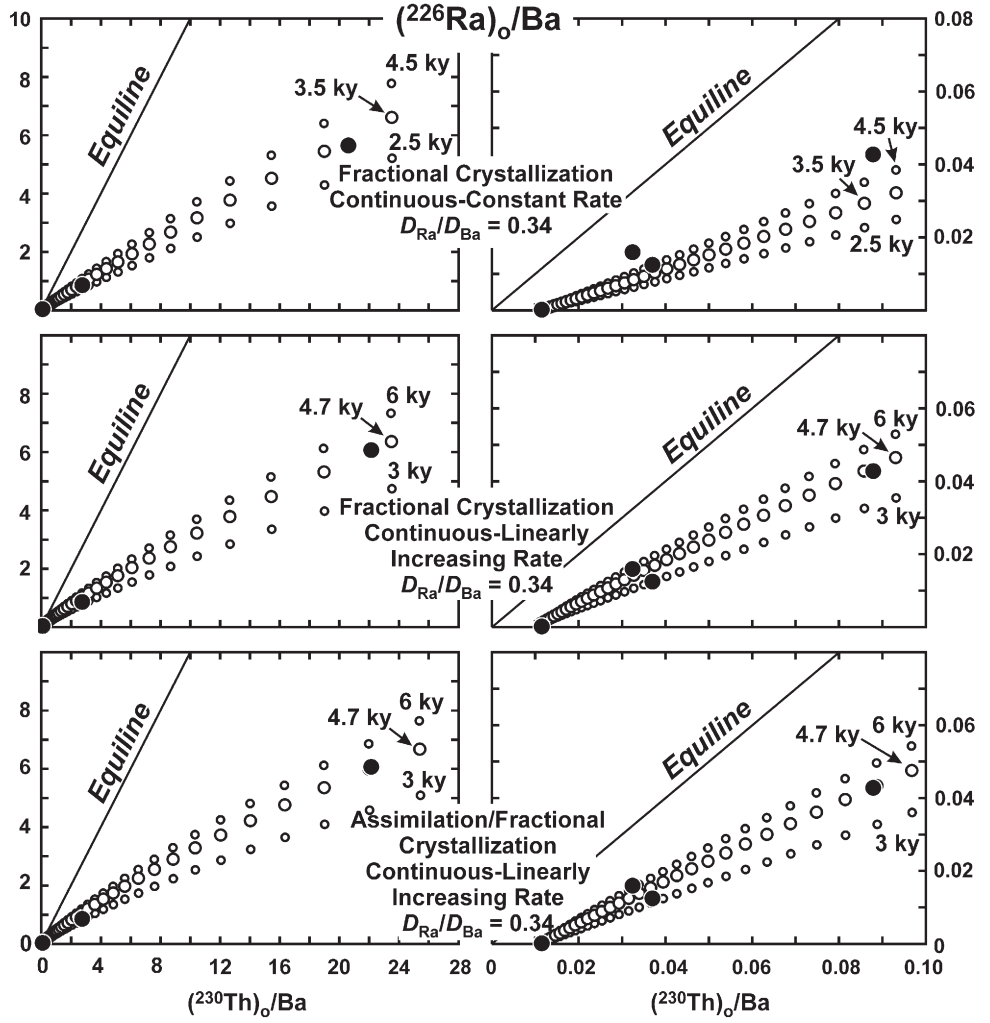

Fig. 9. Continuous differentiation time scale model results for the Fogo A glass separates. Solid circles represent the age corrected measured values, large open circles represent the model results, and small open circles represent model results of time scales different from the best-fit time scale for each respective model (shown for comparison). All models use a D_{Ra}/D_{Ba}=0.34. Crystallization increments of 0.01% were used in the models, but only 1% fractional crystallization (or assimilation–fractional crystallization) increments are illustrated. The continuous models with linearly increasing rate of fractional crystallization (FC) and assimilation–fractional crystallization describe the data equally well and predict identical time scales of differentiation (4.7 ky), whereas the continuous FC with constant rate FC poorly describes the intermediate (^{226}Ra)$_o$/Ba samples. AFC parameters are the same as those in Fig. 7, and Ba=20 ppm and (^{226}Ra/^{230}Th)=1 in the assimilant. The syenite assimilant composition used is based on data from Widom et al. (1993); see text for details.

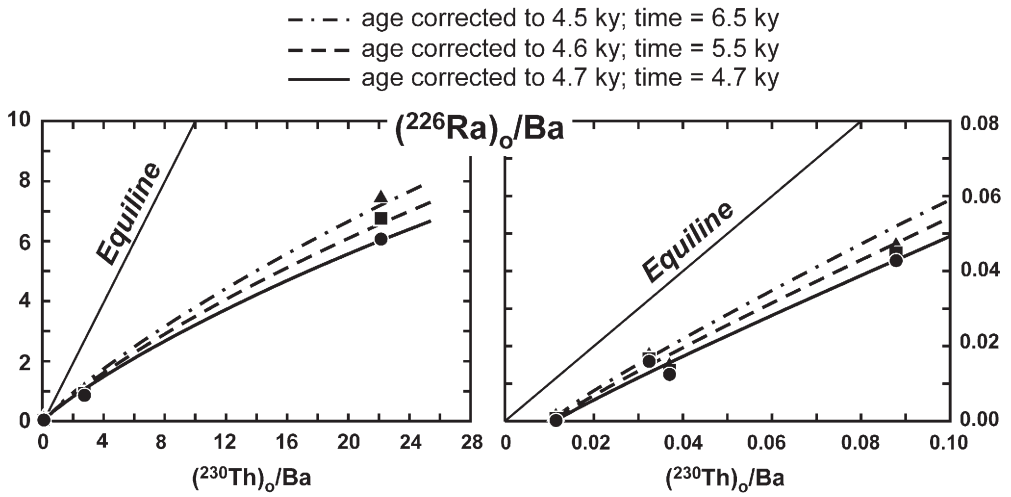

Fig. 10. Model results for continuous AFC with a linearly increasing rate of fractionation for the Fogo A glass separates. The (^{230}Th)/Ba and (^{226}Ra)/Ba ratios have been eruption age corrected to 4.7 ky (the maximum allowable age based on our lowest (^{226}Ra) sample), 4.6 ky, and 4.5 ky. Decreasing the assumed eruption age results in an increased slope of the age corrected data, and thus the modeled time scale of differentiation increases. Modeled fractionation time scales based on a 4.7 ka eruption age thus represent a *minimum* pre-eruptive magma residence time.

time scale. It is interesting to note that the best-fit model is obtained with a D_{Ra}/D_{Ba} ratio = 0.34, despite this ratio having been calculated entirely independently from the fractionation model itself (see Section 5.1.1).

Table 4
Fogo A time scale results as function of variable AFC conditions

D_{Ra}/D_{Ba}	r[a]	(^{226}Ra/^{230}Th)$_o$ of assimilant	Calculated time scale (y)	Comments
0.34	**0.075**	**1**	**4700**	Preferred model discussed in text and shown in Fig. 9
0.34	0.075	2	4200	
0.34	0.075	10	<50	Cannot fit data, see Fig. 11
0.34	0.075	0.5	5000	
0.34	0.075	0.1	5200	
0.34	0.15	1	5000	
0.34	0.75	1	18000	Extremely poor fit to data, see Fig. 11
0.34	0.0352	1	4700	
0.34	0.0075	1	4700	Model fits data well, however Ba/Th ratio of assimilant needs to be decreased from 0.5 to 0.005 in order to explain most evolved trachyte (Ba/Th in syenites = 0.08 − 20; Widom et al., 1993)

Note: Model used for these calculations is the AFC continuous-linearly increasing rate model discussed in the text and shown in Fig. 9. Bold data represent our preferred model.

[a] r = rate of assimilation/rate fractional crystallization.

Given these results and the similarity in the modeled time scales of the continuous, linearly increasing rate of fractional crystallization model and the AFC model, we conclude that prolonged crystallization rather than assimilation is the dominant control on the ^{226}Ra–^{230}Th disequilibria in the Fogo A magma. The effects of AFC appear to be swamped by crystallization of sanidine, such that removal of sanidine, and therefore Ra, from the liquid strongly overrides any effects of assimilation on the ^{226}Ra–^{230}Th–Ba systematics.

The continuous replenishment model that we have described should be considered an end-member model, and other scenarios could be envisioned for the genesis of the Fogo magmatic system. For example, another geologically viable end-member model is one in which instantaneous filling of the chamber and subsequent prolonged fractional crystallization of the magma is simulated. However, the most evolved liquid in both of these end-member models would experience identical fractionation and ingrowth/decay histories and the instantaneous fill model would thus be constrained to produce the same calculated duration of fractionation as the continuous fill model in order to produce the observed ^{226}Ra–^{230}Th–Ba characteristics of the most evolved sample. However, the instantaneous fill model would produce a shallower slope because the less evolved magmas also would have to evolve over this extended residence time, and thus an instantaneous fill model cannot simultaneously reproduce the compositions of the most and least evolved samples.

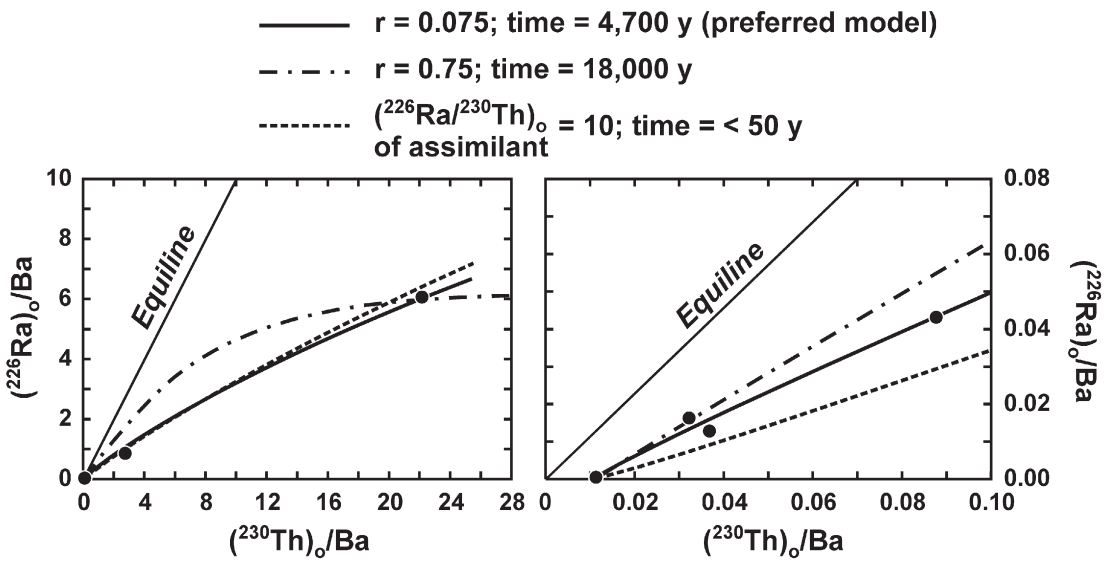

Fig. 11. Model results for continuous AFC with a linearly increasing rate of fractionation for the Fogo A glass separates. The best-fit curve (solid line) corresponds to the preferred model described in the text. However, this curve is also representative of the shapes of the other calculated models shown in Table 4 with the exception of the (^{226}Ra/^{230}Th) ratio of the assimilant curve and the rate of assimilation to rate of the extreme models (dashed curves) that produce very poor fits to the Fogo A data.

5.3. Differentiation time scales and eruptive history of the Fogo Volcano

Approximately 4200 years elapsed between the Fogo A and Fogo 1563 eruptions, during which time three intervening eruptions occurred, including Fogo B, C and D (Booth et al., 1978). The only eruption age available for these deposits is a calibrated radiocarbon age of ~3.8 ka for the Fogo B deposit. Again, this must be considered a maximum eruption age. Therefore, the

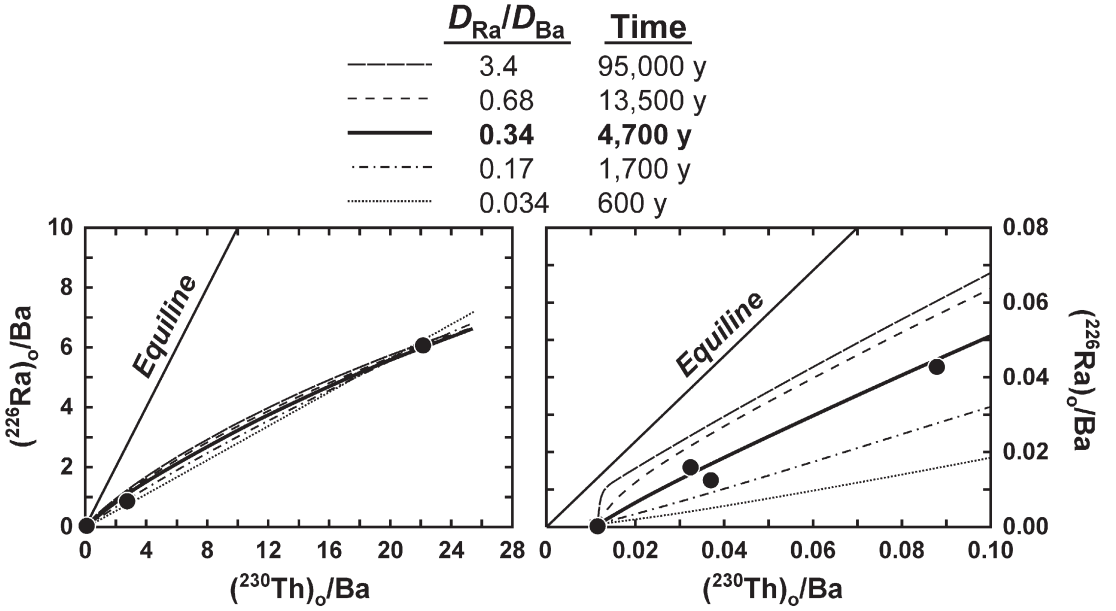

Fig. 12. Model results for continuous AFC with a linearly increasing rate of fractionation for the Fogo A glass separates. Each curve corresponds to a different D_{Ra}/D_{Ba} ratio used in the model. Modeled time scales are highly sensitive to the D_{Ra}/D_{Ba} ratio. Note that the models using D_{Ra}/D_{Ba} ratios higher or lower than 0.34 do not produce good fits to the data.

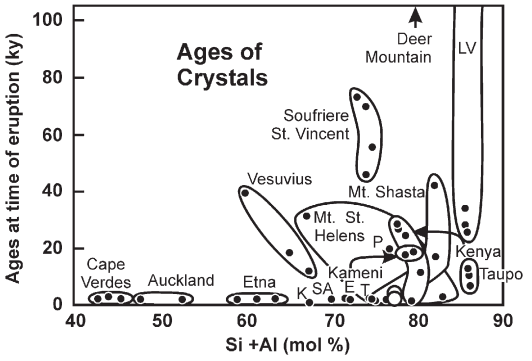

Fig. 13. Plot of crystal ages versus Si+Al contents (mol%) of the bulk rock (after Hawkesworth et al., 2000). Most of the crystal ages are interpreted from internal ^{238}U–^{230}Th mineral isochrons from recent volcanic rocks, whereas the Fogo deposits from this study are liquid ages represented by the open circles. The magma residence times we report for the Fogo deposits are shorter than many of the crystal ages reported in bulk rocks with similar Si+Al contents. E denotes Mt. Erebus, Antarctica; K is Kilauea, Hawaii (1955); P is Parinacota, Chile; T is Toba Tuff; SA is Sangeang Api, Indonesia. Data from Volpe and Hammond (1991), Reagan et al. (1992), Volpe (1992), Bourdon et al. (1994), Reid et al. (1997), Black et al. (1998a,b), Davies and Halliday (1998), Heath et al. (1998), Bourdon et al. (2000), Cooper et al. (2001), Heumann and Davies (2002), Heumann et al. (2002), Vasquez and Reid (2002), Turner et al. (2003).

most recent eruption prior to Fogo 1563 (Fogo D) took place within 3.3 ky of Fogo 1563. Our modeled fractionation duration of ~50–80 years for the Fogo 1563 magma is consistent with the Fogo 1563 magma having been emplaced at a high level relatively shortly before eruption, and does not require that a significant volume of magma remained in the chamber following the Fogo D eruption. Based on geochemical and mineralogical variations, Storey (1981) suggested that the five most recent eruptions of Fogo volcano (Fogo A through Fogo 1563 A.D.) represent successive samples of a single magma body. This interpretation is inconsistent with our modeled time scale of fractionation for the Fogo 1563 A.D. magma.

The most recent eruption of Fogo volcano preceding that of Fogo A took place ~15,200 y BP (~10,600 years prior to the Fogo A eruption; Moore, 1991). Our modeled differentiation duration for the Fogo A magma is ~4.7 ky, allowing (although not requiring) that the magma chamber was fully emptied during the 15.2 ky caldera forming eruption and that a new magma entered the system after the 15.2 ky caldera forming eruption.

Chemical composition, volume and tectonic regime are but a few of the factors that could influence the time scales over which fractionation will take place in a magmatic system. Our time scale results for the Fogo A magmatic system are generally consistent with results from other evolved alkaline magmatic systems. Residence times based on U-series data of evolved trachytes from Longonot volcano, Kenya (eruptive volume of 18–20 km^3; Evans, 1999; Rogers et al., 2004) and Puy de Dôme, French Massif Central (eruptive volume of 0.3 km^3; Condomines, 1997) have been modeled at less than a few centuries up to a few thousand years. Residence time estimates for evolved phonolites of ~4–10 ky from Laacher See, east Eifel Germany (eruptive volume of ~6 km^3; Bourdon et al., 1994, Schmitt, 2006) and ~3 ky for Mt. Erebus, Antarctica (eruptive volume <1 km^3; Reagan et al., 1992) are also similar to the results presented here for the Fogo volcano (eruptive volumes 0.14 km^3 and 0.7 km^3).

The Fogo residence times are also similar to some of the crystal residence times of similarly evolved (i.e. similar Si+Al mol%) calc-alkaline magmas summarized by Hawkesworth et al. (2000), but are much shorter than others (Fig. 13). Most of the crystal residence times illustrated in Fig. 13 are based on internal ^{238}U–^{230}Th mineral isochrons, whereas the Fogo residence times are based either on whole rock or glass separate data. The residence time differences could be at least partially accounted for by the different methods with which the time scales were obtained. Magma fractionation time scales based on mineral separate data may be biased due to incorporation of old xenocrysts or by complex crystallization histories (Charlier and Zellmer, 2000).

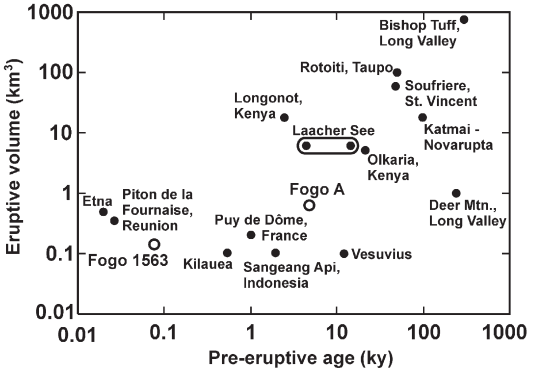

Fig. 14. Plot of eruptive volume versus pre-eruptive magma age for volcanic deposits associated with individual eruptive events. Most of the pre-eruptive ages are based on U–Th mineral isochron results. These deposits span a wide range in chemical compositions and are associated with highly varied tectonomagmatic settings. Time scale data from Bourdon et al. (1994), Condomines et al. (1995), Condomines (1997), Black et al. (1998b), Davies and Halliday (1998), Heath et al. (1998), Cooper et al. (2001), Heumann et al. (2002), Heumann and Davies (2002), Charlier et al. (2003), Reagan et al. (2003), Turner et al. (2003), Rogers et al. (2004), Sigmarsson et al. (2005), Schmitt (2006).

The relationship between fractionation duration and eruptive volume exhibited between the Fogo 1563 and Fogo A magmas suggests that at least for Fogo, larger volume eruptions are characterized by longer durations of fractionation. The Fogo A deposit consists of 0.6–0.7 km^3 DRE of trachytic pumice lapilli erupted after ~4.7 ky of magmatic fractionation, whereas the Fogo 1563 eruption produced only 0.14 km^3 DRE resulting from 50–80 y of magmatic differentiation. Whether or not such a relationship is representative of magmatic systems in general is unknown at this time. The data in Fig. 14 span a wide range in magma compositions, from different tectonic settings, and have residence times calculated by a variety of means; significant scatter would therefore be expected. Although there is indeed significant scatter, an overall positive correlation between eruptive volume and pre-eruptive magma fractionation time scale is suggested. Further studies similar to the present one, that determine liquid rather than crystal ages, should help to constrain potential relationships between magma residence times and eruptive magnitude if they exist, and ultimately allow for more meaningful comparisons of magma residence times in volcanic systems from different compositional and tectonic regimes.

6. Conclusion

The chemical and isotopic variations exhibited by the Fogo 1563 and Fogo A deposits are interpreted to result from prolonged fractionation of trachytic magmas over time periods of 50–80 y and ~4.7 ky, respectively. The modeled time scales of fractionation are essentially independent of the type of continuous crystallization model used (e.g., constant rate, linearly increasing rate, AFC). However the time scales are strongly dependent on the relative bulk D's used for Ba and Ra. The elastic strain model predicts $D_{Ra}/D_{Ba}<1$ in the Fogo magmas. For a given D_{Ra}/D_{Ba}, we are able to place firm constraints on the time scales of fractionation, but improved, experimentally determined, D_{Ra}/D_{Ba} for evolved alkaline magmatic systems will allow more rigorous time scales to be estimated.

Our approach is unique in that our time scale estimates are based on high precision analyses of ^{226}Ra–^{230}Th–^{238}U disequilibria on volcanic glass separates and crystal-poor whole rocks, rather than combined whole rock–mineral separate analyses. This provides an ideal proxy for the chemical and isotopic variation of a liquid over the course of its differentiation, independent of the potential complications such as prolonged and/or episodic crystal growth associated with mineral separate data (Hughes and Hawkesworth, 1999; Charlier and Zellmer, 2000). The high precision with which U-series disequilibria can currently be measured affords the opportunity to obtain meaningful time scale results based solely on glass separates, avoiding the potential complex crystallization histories of mineral separates. However, the precision with which these time scales can be modeled is currently hindered by the lack of precise knowledge of the relative partitioning of Ra and Ba in such systems. This study highlights the potential utility of experimentally determined D_{Ra} in evolved magmatic systems in the future.

Finally, we note that the $^{226}Ra/^{230}Th$ data for the Fogo A trachytes places an upper limit on the eruption age for Fogo A of 4.73 ky. Previously determined ^{14}C ages for this eruption were significantly older and highly variable. Our new results suggest that ^{14}C dates for Fogo volcano may provide erroneously old ages due to the incorporation of magmatic CO_2 in local vegetation.

Acknowledgements

M. Horan and T. Mock are thanked for their assistance with all isotope analyses at the Department of Terrestrial Magnetism. Stephen Blake and two anonymous reviewers provided thorough and insightful comments on an earlier draft. Financial support for this project was provided by the Geological Society of America (student research awards to D.S. 2000 and 2001), Sigma Xi (Grants-in-Aid of research awards to D.S. 2000 and 2001) and National Science Foundation (NSF EAR 0207529 and MRI EAR 0116033 awarded to E.W. and NSF EAR 0003359 to A.P.).

References

Allegre, C.J., Condomines, M., 1976. Fine chronology of volcanic processes using ^{238}U–^{230}Th systematics. Earth Planet. Sci. Lett. 28, 395–406.

Black, S., Macdonald, R., Barreiro, B.A., Dunkley, P.N., Smith, M., 1998a. Open system alkaline magmatism in northern Kenya: evidence from U-series disequilibria and radiogenic isotopes. Contrib. Mineral. Petrol. 131, 364–378.

Black, S., Macdonald, R., De Vivo, B., Kilburn, C.R.J., Rolandi, G., 1998b. U-series disequilibria in young (A.D. 1944) Vesuvius rocks: preliminary implications for magma residence times and volatile addition. J. Volcanol. Geotherm. Res. 82, 97–111.

Blake, S., Rogers, N., 2005. Magma differentiation rates from ($^{226}Ra/^{230}Th$) and the size and power output of magma chambers. Earth Planet. Sci. Lett. 236, 654–669.

Blundy, J., Wood, B., 1991. Crystal-chemical controls of the partitioning of Sr and Ba between plagioclase feldspar, silicate melts, and hydrothermal solutions. Geochim. Cosmochim. Acta 55, 193–209.

Blundy, J., Wood, B., 1994. Prediction of crystal–melt partition coefficients from elastic moduli. Nature 372, 452–454.

Blundy, J., Wood, B., 2003. Mineral–melt partitioning of uranium, thorium and their daughters. Rev. Mineral. Geochem. 52, 59–123.

Booth, B., Croasdale, R., Walker, G., 1978. A quantitative study of five thousand years of volcanism on São Miguel, Azores. Philos. Trans. R. Soc. Lond. 288, 271–319.

Bourdon, B., Zindler, A., Wörner, G., 1994. Evolution of the Laacher See magma chamber; evidence from SIMS and TIMS measurements of U–Th disequilibria in minerals and glasses. Earth Planet. Sci. Lett. 126, 75–90.

Bourdon, B., Wörner, G., Zindler, A., 2000. U-series evidence for crustal involvement and magma residence times in the petrogenesis of Parinacota volcano, Chile. Contrib. Mineral. Petrol. 139, 458–469.

Bursik, M.I., Sparks, R.S.J., Gilbert, J.S., Carey, S.N., 1992. Sedimentation of tephra by volcanic plumes: I. Theory and its comparison with a study of the Fogo A plinian deposit, São Miguel (Azores). Bull. Volcanol. 54, 329–344.

Charlier, B., Zellmer, G., 2000. Some remarks on U–Th mineral ages from igneous rocks with prolonged crystallisation histories. Earth Planet. Sci. Lett. 183, 457–469.

Charlier, B., Peate, D.W., Wilson, C.J.N., Lowenstern, J.B., Storey, M., Brown, S.J.A., 2003. Crystallisation ages in coeval silicic magma bodies: ^{238}U–^{230}Th disequilibrium evidence from Rotoiti and Earthquake Flat eruption deposits, Taupo Volcanic Zone, New Zealand. Earth Planet. Sci. Lett. 206, 441–457.

Condomines, M., 1997. Dating recent volcanic rocks through ^{230}Th–^{238}U disequilibrium in accessory minerals: example of the Puy de Dôme (French Massif Central). Geology 25, 375–378.

Condomines, M., Tanguy, J.C., Michaud, V., 1995. Magma dynamics at Mt. Etna: constraints from U–Th–Ra–Pb radioactive disequilibria and Sr isotopes in historical lavas. Earth Planet. Sci. Lett. 132, 25–41.

Cooper, K.M., Reid, M.R., 2003. Re-examination of crystal ages in recent Mount St. Helens lavas: implications for magma reservoir processes. Earth Planet. Sci. Lett. 213, 149–167.

Cooper, K.M., Reid, M.R., Murrell, M.T., Clague, D.A., 2001. Crystal and magma residence at Kilauea Volcano, Hawaii; ^{230}Th–^{226}Ra dating of the 1955 East Rift eruption. Earth Planet. Sci. Lett. 184, 703–718.

Davies, G.R., Halliday, A.N., 1998. Development of the Long Valley rhyolitic magma system; strontium and neodymium isotope evidence from glasses and individual phenocrysts. Geochim. Cosmochim. Acta 62, 3561–3574.

Evans, P., 1999. A U-series disequilibrium study of the Longonot trachyte magma chamber, Kenya. Ph.D. thesis, The Open Univ., Milton Keynes.

Gandino, A., Guidi, M., Merlo, C., Mete, L., Rossi, R., Zan, L., 1985. Preliminary model of the Ribeira Grande geothermal field (Azores Islands). Geothermics 14, 91–105.

Hawkesworth, C.J., Blake, S., Evans, P., Hughes, R., MacDonald, R., Thomas, L.E., Turner, S.P., Zellmer, G., 2000. Time scales of crystal fractionation in magma chambers; integrating physical, isotopic and geochemical perspectives. J. Petrol. 41, 991–1006.

Hawkesworth, C.J., George, R., Turner, S.P., Zellmer, G., 2004. Time scales of magmatic processes. Earth Planet. Sci. Lett. 218, 1–16.

Heath, E., Turner, S.P., Macdonald, R., Hawkesworth, C., vanCalsteren, P., 1998. Long magma residence times at an island arc volcano (Soufriere, St. Vincent) in the Lesser Antilles evidence from ^{238}U–^{230}Th isochron dating. Earth Planet. Sci. Lett. 160, 49–63.

Heumann, A., Davies, G.R., 2002. U–Th disequilibrium and Rb–Sr age constraints on the magmatic evolution of peralkaline rhyolites from Kenya. J. Petrol. 43, 557–577.

Heumann, A., Davies, G.R., Elliott, T., 2002. Crystallization history of rhyolites at Long Valley, California, inferred from U-series and Rb–Sr isotope systematics. Geochim. Cosmochim. Acta 66, 1821–1837.

Hughes, R.D., Hawkesworth, C.J., 1999. The effects of magma replenishment processes on ^{238}U–^{230}Th disequilibrium. Geochim. Cosmochim. Acta 63, 4101–4110.

Jicha, B.R., Singer, B.S., Beard, B.L., Johnson, C.M., 2005. Contrasting timescales of crystallization and magma storage beneath the Aleutian Island arc. Earth Planet. Sci. Lett. 236, 195–210.

Johansen, T.S., Hauff, F., Hoernle, K., Klügel, A., Kokfelt, T.F., 2005. Basanite to phonolite differentiation within 1550–1750 yr: U–Th–Ra isotopic evidence from the A.D. 1585 eruption on La Palma, Canary Islands. Geology 33, 897–900.

Mahood, G., Hildreth, W., 1983. Large partition coefficients for trace elements in high-silica rhyolites. Geochim. Cosmochim. Acta 47, 11–30.

Moore, R.B., 1990. Volcanic geology and eruption frequency, São Miguel, Azores. Bull. Volcanol. 52, 602–614.

Moore, R.B., 1991. Geology of three Late Quaternary stratovolcanoes on São Miguel, Azores. U.S.G.S Bull. 1900, 1–46.

Moore, R.B., Rubin, M., 1991. Radiocarbon dates for lava flows and pyroclastic deposits on São Miguel, Azores. Radiocarbon 33, 151–164.

Pasquier-Cardin, A., Allard, P., Ferreira, T., Hatte, C., Coutinho, R., Fontugne, M., Jaudon, M., 1999. Magma-derived CO_2 emissions recorded in ^{14}C and ^{13}C content of plants growing in Furnas caldera, Azores. J. Volcanol. Geotherm. Res. 92, 195–207.

Pietruszka, A.J., Carlson, R.W., Hauri, E.H., 2002. Precise and accurate measurement of ^{226}Ra–^{230}Th–^{238}U disequilibria in volcanic rocks using plasma ionization multicollector mass spectrometry. Chem. Geol. 188, 171–191.

Pietruszka, A.J., Hauri, E.H., Carlson, R.W., Garcia, M.O., 2006. Remelting of recently depleted mantle within the Hawaiian plume inferred from the ^{226}Ra–^{230}Th–^{238}U disequilibria of Pu'u'Ō'ō eruption lavas. Earth Planet. Sci. Lett. 244, 155–169.

Reagan, M.K., Cashman, K.V., Volpe, A.M., 1992. ^{238}U–^{230}Th-series chronology of phonolite fractionation at Mount Erebus, Antarctica. Geochim. Cosmochim. Acta 56, 1401–1407.

Reagan, M.K., Ball, L., Cheng, H., Edwards, R.L., Erich, J., Layne, G., Sims, K.W.W., Thomas, R.B., 2003. Time-scales of differentiation from mafic parents to rhyolite in North American continental arcs. Chem. Geol. 44, 1703–1726.

Reagan, M., Tepley, F.J., Gill, J.B., Wortel, M., Hartman, B., 2005. Rapid time scales of basalt to andesite differentiation at Anatahan volcano, Mariana Islands. J. Volcanol. Geotherm. Res. 146, 171–183.

Reid, M.R., Coath, C.D., Harrison, M., McKeegan, K.D., 1997. Prolonged residence times for the youngest rhyolites associated with the Long Valley Caldera: ^{230}Th–^{238}U ion microprobe dating of young zircons. Earth Planet. Sci. Lett. 150, 27–39.

Reimer, P.J., Baillie, M.G.L., Bard, E., Bayliss, A., Beck, J.W., Bertrand, C.J.H., Blackwell, P.G., Buck, C.E., Burr, G.S., Cutler, K.B., Damon, P.E., Edwards, R.L., Fairbanks, R.G., Friedrich, M., Guilderson, T.P., Hogg, A.G., Hughen, K.A., Kromer, B., McCormac, G., Manning, S., Ramsey, C.B., Reimer, R.W., Remmele, S., Southon, J.R., Stuiver, M., Talamo, S., Taylor, F.W., van der Plicht, J., Weyhenmeyer, C.E., 2004. IntCal04 terrestrial radiocarbon age calibration, 0–26 Cal Kyr BP. Radiocarbon 46, 1029–1058.

Rhodes, J.M., 1996. Geochemical stratigraphy of lava flows sampled by the Hawaii Scientific Drilling Project. J. Geophys. Res. 101, 11729–11746.

Rogers, N.W., Evans, P.J., Blake, S., Scott, S.C., Hawkesworth, C.J., 2004. Rates and time scales of fractional crystallization from ^{238}U–^{230}Th–^{226}Ra disequilibria in trachyte lavas from Longonot volcano, Kenya. J. Petrol. 45, 1747–1776.

Rogers, N.W., Thomas, L.E., Macdonald, R., Hawkesworth, C.J., Mokadem, F., 2006. ^{238}U–^{230}Th disequilibrium in recent basalts and dynamic melting beneath the Kenya rift. Chem. Geol. 234, 148–168.

Schmitt, A.K., 2006. Laacher See revisited: high-spatial-resolution zircon dating indicates rapid formation of a zoned magma chamber. Geology 34, 597–600.

Shannon, R.D., 1976. Revised effective ionic radii and systematic studies of interatomic distances halides and chalcogenides. Acta Crystallogr. A32, 751–767.

Shotton, F.W., Blundell, D.J., Williams, R.E.G., 1968. Birmingham University radiocarbon dates II. Radiocarbon 10, 200–206.

Shotton, F.W., Blundell, D.J., Williams, R.E.G., 1969. Birmingham University radiocarbon dates III. Radiocarbon 11, 263–270.

Sigmarsson, O., Condomines, M., Bachèlery, P., 2005. Magma residence time beneath Piton de la Fournaise Volcano, Reunion Island, from U-series disequilibria. Earth Planet. Sci. Lett. 234, 223–234.

Snyder, D.C., Widom, E., Pietruszka, A.J., Carlson, R.W., 2004. The role of open-system processes in the development of silicic magma chambers: a chemical and isotopic investigation of the Fogo A trachyte deposit, São Miguel Azores. J. Petrol. 45, 723–738.

Storey, M., 1981. Trachytic pyroclastics from Agua de Pao volcano, São Miguel, Azores: evolution of a magma body over 4000 years. Contrib. Mineral. Petrol. 78, 423–432.

Storey, M., Wolff, J.A., Norry, M.J., Marriner, G.F., 1989. Origin of hybrid lavas from Agua de Pao volcano, São Miguel, Azores. In: Saunders, A.D., Norry, M.J. (Eds.), Magmatism in the Ocean Basins. Geol. Soc. Spec. Pub., vol. 42, pp. 161–180.

Turner, S., Foden, J., George, R., Evans, P., Varne, R., Elburg, M., Jenner, G., 2003. Rates and processes of potassic magma generation beneath Sangeang Api volcano, east Sunda arc, Indonesia. Chem. Geol. 44, 491–515.

Vasquez, J.A., Reid, M.R., 2002. Constraining the timing of magmatic evolution in the Youngest Toba Tuff rhyolite through dating of zoning in allanite. Geochim. Cosmochim. Acta 66 (15A), 802.

Volpe, A.M., 1992. ^{238}U–^{230}Th–^{226}Ra disequilibrium in young Mt. Shasta andesites and dacites. J. Volcanol. Geotherm. Res. 53, 227–238.

Volpe, A.M., Hammond, P.E., 1991. ^{238}U–^{230}Th–^{226}Ra disequilibria in young Mount St. Helens rocks; time constraint for magma formation and crystallization. Earth Planet. Sci. Lett. 107, 475–486.

Walker, G.P.L., Croasdale, R., 1970. Two Plinian-type eruptions in the Azores. J. Geol. Soc. (Lond.) 127, 17–55.

Watanabe, S., Widom, E., Wallenstein, N., Snyder, D., 2005. The evolution of chemically zoned trachytic deposits: comparisons of Fogo A and Fogo 1563AD, São Miguel, Azores. Geochim. Cosmochim. Acta 69 (10), 245.

Widom, E., Schmincke, H.-U., Gill, J., 1992. Processes and time scales in the evolution of a chemically zoned trachyte: Fogo A, São Miguel, Azores. Contrib. Mineral. Petrol. 111, 311–328.

Widom, E., Gill, J., Schmincke, H.-U., 1993. Syenite nodules as a long-term record of magmatic activity in Agua de Pao volcano, São Miguel, Azores. Chem. Geol. 34, 929–953.

Williams, R.W., Gill, J.B., Bruland, K.W., 1986. Ra–Th disequilibria systematics: time scale of carbonatite magma formation at Oldoinyo Lengai volcano, Tanzania. Geochim. Cosmochim. Acta 50, 1249–1259.

Wolff, J.A., Storey, M., 1983. The volatile component of some pumice-forming alkaline magmas from the Azores and Canary Islands. Contrib. Mineral. Petrol. 82, 66–74.

Zellmer, G.F., Turner, S.P., Hawkesworth, C.J., 2000. Time scales of destructive plate margin magmatism: new insights from Santorini, Aegean Volcanic Arc. Earth Planet. Sci. Lett. 174, 265–281.